Influence of film thickness on the physical properties of manganite heterojunctions

Weiwei Gao,[1] Xuan Sun,[2] Jing Wang,[1] Dashan Shang,[1] Baogen Shen,[1] and Jirong Sun[1,a)]
[1]*Beijing National Laboratory for Condensed Matter Physics and the Institute of Physics, Chinese Academy of Sciences, Beijing 100190, People's Republic of China*
[2]*Department of Physics, Beihang University, Beijing 100080, People's Republic of China*

(Received 10 November 2010; accepted 6 December 2010; published online 20 January 2011)

Rectifying and photoelectronic properties of the $La_{0.67}Ba_{0.33}MnO_3/SrTiO_3$:Nb junctions with the film thickness from $d=0.5$ to 30 nm have been systematically studied. It is found that the electronic transport of the junction is dominated by quantum tunneling or thermoionic emission when film thickness is below or above 1 nm. The rectifying ratio and ideality factor, correspondingly, experience a sudden change as film thickness grows from 0.5 to 1 nm and a smooth variation with film thickness above 1 nm. The threshold film thickness for the establishment of a mature depletion layer is therefore 1 nm. The photoemission properties of the junctions also exhibit a strong dependence on film thickness. As experimentally shown, the photocurrent vanishes in the zero thickness limit, and grows rapidly with the increase in film thickness until $d=6$ nm, where a maximal photocurrent of ~ 770 nA/mm^2 under the irradiance of the laser of 5 mW and 532 nm is obtained. After this maximum, an increase-to-decrease turning appears with further increasing film thickness. Taking into account the finite diffusion distance of the photocarriers and the strain-enhanced charge trapping in ultrathin film junctions, a theoretical description that well reproduces the experiment results can be obtained, which reveals the severe depression of finite diffusion distance of the extra carriers on photocurrent. The maximal diffusion distance thus obtained is ~ 3.5 nm. Similar analyses have been performed for the $La_{0.67}Ca_{0.33}MnO_3/SrTiO_3$:Nb junctions, and the corresponding diffusion distance there is ~ 1.5 nm. © *2011 American Institute of Physics*. [doi:10.1063/1.3537916]

I. INTRODUCTION

The colossal magnetoresistance and related effects in hole-doped manganites have received remarkable attention in nearly the last two decades. After great efforts, both theoretical and experimental, it has been well established that competitive mechanisms such as double exchange, superexchange, and Coulomb repelling coexist in the manganites, and it is the unbalance of the different interactions, under external stimuli, that results in the dramatic magnetoresistance effects.[1] It is obvious that if parts of the distinctive features of the manganite can be inherited by the manganite-based heterostructures, diverse properties absent in the conventional junctions are possible. Indeed, interesting phenomena such as magnetic field-dependent rectifying characteristics and photovoltaic effect have been observed in manganite junctions.[2–4] Emergent effects associated with interfacial decorations are also detected, for example, the enhancement of interface ferromagnetism in the $La_{0.6}Sr_{0.4}MnO_3/LaMnO_3/SrTiO_3$ structure, the two-process-featured rectifying behavior in the $La_{0.67}Ca_{0.33}MnO_3/LaMnO_3/SrTiO_3$:Nb junctions,[5] and the growth of the interfacial potential after the introduction of a $SrMnO_3$ monolayer in the $La_{0.7}Sr_{0.3}MnO_3/SrTiO_3$:Nb junction.[6]

We noted that most of the previous works focused on the junctions composed of the manganite films thicker than 150 nm. However, thin film junctions have the characters of their own and deserve special attention. At first, the effects of heterointerface are highlighted in thin film junctions. As well known, the physical properties of the junctions have a close relation to interfacial states. The latter is generally different from the interior ones. For instance, the Curie temperature and magnetic polarization are significantly low at the interface,[7] the manganite-substrate interface is insulating at low temperatures,[8] and the electron transport across the grain boundaries proceeds in the manner of quantum tunneling.[9] It is also found that small grain sizes[10] or strong lattice strains[11] can completely depress the charge ordering, which is the most typical feature of some half-doped manganites. These works clearly demonstrate the importance of interface/surface for the manganites. Considering the highlighting of the role of heterointerfaces, distinctive behaviors are expected in ultrathin film junctions. Second, the interfacial states, depletion width, and electronic processes in the ultrathin film junctions may be considerably different from those of the thick ones. As well established, the establishment of the depletion layer requires the charge exchange between the p and n poles of the junctions, to balance the difference of the Fermi levels of the two components. For the ultrathin junction, however, the number of the holes may be insufficient to form a depletion layer similar to that of the thick junctions. It is the interfacial states that participate in the build-up of the junction, thus determine the properties of the junction. Third, the nonequilibrium charge carriers could be-

a)Electronic mail: jrsun@g203.iphy.ac.cn.

have differently in thin film junctions. Take the kinetic/dynamic behavior of the charge carriers as an example.[12,13] When the diffusion distance of the photocarriers is comparable or smaller than film thickness, size effect may occur, resulting in dramatic changes in the photovoltaic properties of the junctions. As we know, the injection, drift and diffusion of charge carriers are important topics of electronics. The knowledge on diffusion distance, mobility, and lifetime of the nonequilibrium carriers is highly desirable for practical application, especially for the designing of manganite-based device structures working via the manipulation of extra carriers. For the typical semiconductor with a carrier concentration of $10^{16}/cm^3$, the diffusion length and lifetime are generally $\sim 10^3$ nm and ~ 10 μs, respectively.[14] Due to strong carrier scattering, the diffusion distance, and lifetime could be extremely short in the manganites. Through the investigation of the photoelectric properties of the junctions of various film thickness, one may get important information about the transient processes. This is particularly meaningful for the manganites because of the presence of strongly coupled spin, charge, orbital, and lattice degrees of freedom. Based on these consideration, in this paper, we performed a systematic study on the $La_{0.67}Ba_{0.33}MnO_3/SrTiO_3$:Nb (LBMO/STON) and $La_{0.67}Ca_{0.33}MnO_3/SrTiO_3$:Nb (LCMO/STON) junctions, focusing on the evolution of the rectifying and photoelectric properties of the junctions with the thickness of the LBMO (LCMO) film. The electronic transport in the junctions undergoes a tunneling to thermal activation evolution as the film thickness increases from 0.5 to 1 nm, leading to a dramatic change in the rectifying properties. As experimentally shown, the photocurrent vanishes in the zero thickness limit, and grows rapidly with the increase in film thickness until $d=6$ nm (2 nm), where a maximal photocurrent of ~ 770 nA/mm^2 (~ 280 nA/mm^2) under irradiance of the laser of 5 mW and 532 nm is obtained for the LBMO (LCMO) junctions. Further increase in film thickness leads to a gradual decrease in photocurrent. Taking into account the change in the activation energy of the charge carrier in ultrathin film junctions and the finite diffusion distance of the photocarriers, a theoretical analysis is presented, which quantitatively reproduces the experiment results.

II. EXPERIMENTAL PROCEDURE

Two series of manganite junctions have been fabricated by growing, via the pulsed laser ablation technique (laser wavelength=248 nm, repetition rate=1 Hz, and fluency =7 J/cm^2) the LBMO and LCMO films, respectively, on (001)-orientated $SrTiO_3$:0.05 wt % Nb (STON) substrates of the dimension of 3×1 mm^2. During the deposition process, the temperature of the substrate was kept at 720 °C, and the oxygen pressure at ~ 60 Pa, for the LBMO films, or ~ 80 Pa, for the LCMO films. The film thickness is $d=0.5$, 1, 2, 4, 6, 15, and 30 nm, controlled by the number of laser pulses. To determine the thickness of ultrathin films, the deposition rate was carefully calibrated: Two standard films, LBMO and LCMO, were first prepared under the above condition, then parts of the film were removed from the substrate by the conventional lithographic technique and the film edge thus formed was measured by an atomic force microscope (AFM). In this way, the correspondence between pulse number and film thickness was established. LBMO and LCMO were chosen because of their different lattice mismatch with the STON substrate, which is $\sim 0.15\%$ for the LBMO films and $\sim 1.2\%$ for the LCMO films. The LBMO/STON junction will be the focus of the present study, while the data of the LCMO/STON junction provides a supplement.

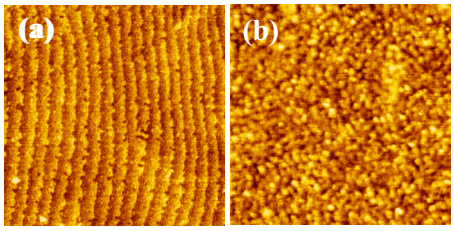

FIG. 1. (Color online) Topology of the manganite films of the LBMO films with the thicknesses of 1 nm (a) and 15 nm (b). The scale of the image is 1×1 μm^2.

As electrodes, two copper pads with a size of 1×1 mm^2 were deposited on manganite films and STON, respectively. Appropriate electric pulses have been applied to the Cu-STON contact to get an Ohmic contact. The contact resistance is ~ 15 Ω for the Cu-STON contact and ~ 200 Ω for the Cu-manganite contact. The current (I)-voltage (V) characteristics of the junctions were measured by a superconducting quantum interference device magnetometer equipped by an electric unit. A laser with a power of 5 mW and the wavelength of $\lambda=532$ nm was used for the photoelectric experiment. The spot size of the light is ~ 0.33 mm in diameter. A Keithley SourceMeter 2611 was used for the acquisition of photocurrent and photovoltage.

III. CURRENT-VOLTAGE CHARACTERISTICS

Figure 1 shows the AFM image of the typical LBMO films. Terrace-featured surface morphology with a step of ~ 0.4 nm is observed in ultrathin films, signifying a layer-by-layer growth of the films. Thick films are also quite smooth, with a topology characterized by densely packed grains of 15 nm. The root mean square roughness varies between ~ 0.2 and ~ 0.3 nm, slightly growing with film thickness.

Figure 2 presents the x-ray diffraction (XRD) spectrum of the LBMO and LCMO films grown on $SrTiO_3$ under the same condition as that of LBMO/STON and LCMO/STON. The XRD peak of the LBMO film, which is very close to that of $SrTiO_3$, is unidentifiable when the film thickness is below 40 nm, and slightly shifts to high angles with the increase in film thickness. The lattice constant is, for example, for the film of 240 nm, ~ 3.925 Å. In contrast, LCMO shows a smaller lattice parameter compared than that of the bulk counterpart.[15] The lattice constant is ~ 3.796 Å for $d=10$ nm (The XRD reflections of the LCMO film are invisible below 10 nm), rapidly increases to 3.808 Å as film thickness grows from 10 to 40 nm, and approaches the saturated value of 3.810 Å above 40 nm. The increase in the lattice constant indicates the relaxation of the tensile strains of the films.

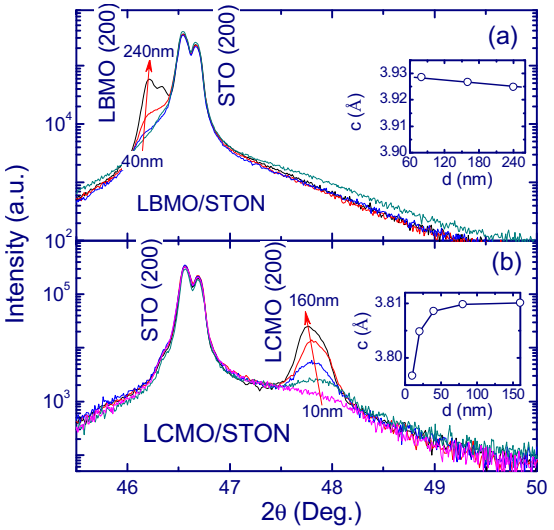

FIG. 2. (Color online) XRD spectra of the LBMO (a) and LCMO (b) films grown on $SrTiO_3$ under the same condition as that of LBMO/STON and LCMO/STON. The inset plot in (b) shows the lattice constant of the LCMO film as a function of film thickness.

Figures 3(a)–3(c) show the current-voltage relations of the typical LBMO/STON junctions of $d=0.5$ nm, 1 nm, and 6 nm, respectively. All of the junctions except for the one of $d=0.5$ nm are excellently rectifying, exhibiting the I-V characteristics obeying the Shockley equation, as demonstrated by the linear log I-V relation under positive biases (directing from manganite film to STON). The rectifying rations at the bias voltage of $|V|=0.3$ V are ~19, ~3600, ~34 500, ~15 000, and ~10 700 for the film thickness of 0.5 nm, 1 nm, 6 nm, 15 nm, and 30 nm, respectively. The junction

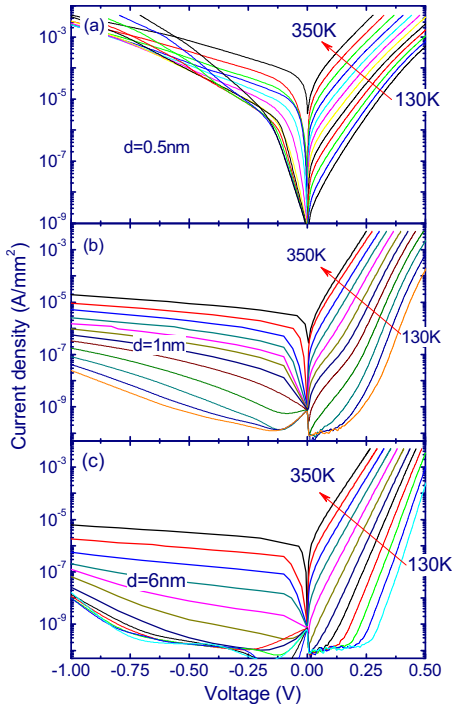

FIG. 3. (Color online) Semilogarithmic current-voltage characteristics of LBMO/STON with the film thicknesses of 0.5 nm (a), 1 nm (b), and 6 nm (c), measured in the temperature range from 130 to 350 K with a temperature step of 20 K. Solid lines are guides for the eye.

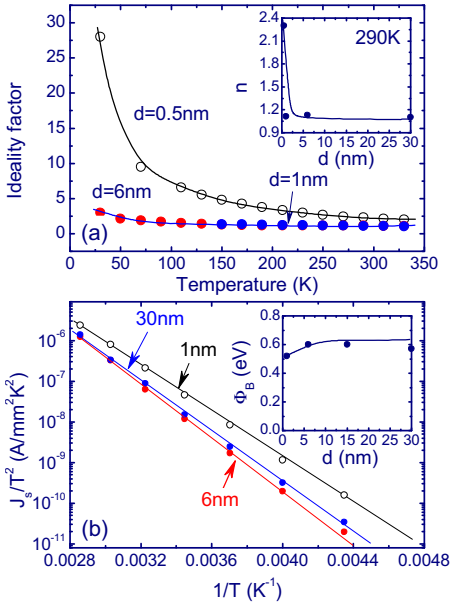

FIG. 4. (Color online) Ideality factor (a) and saturation current (b) as functions of temperature are also presented. Inset plots in (a) and (b) show the ideality factor-film thickness and the interfacial barrier-film thickness relations, respectively. Solid lines are guides for the eye.

resistance at the ambient temperature is $\sim 1\times 10^3$ Ω, $\sim 1.2\times 10^4$ Ω, and $\sim 3\times 10^5$ Ω, respectively, for the film thicknesses of 0 nm, 0.5 nm, and 1 nm, and above 10^6 Ω for other junctions (junction area $=1\times 1$ mm^2). These results reveal the development of the mature depletion layer even for the film of 1 nm.

Based on the analysis of the I-V characteristics, the ideality factor n of the junctions can be obtained [Fig. 4(a)]. It is considerably large for the junction of $d=0.5$, ~2.3 at 290 K and ~6.7 at 110 K. A quantitative analysis shows a simple relation: $1/n \approx -0.01+0.0015T$, marked by the solid curve in the inset plot in Fig. 4(a). According to the semiconductor theory, there are two factors that affect n. The first one is inhomogeneous junction interface and the second one is electric leakage. The latter could be the main reason for the unordinary ideality factor of the present junction in the present case. In fact, the $1/T$ dependence of n indicates the temperature independence of the ln(I)-V slope, which is a signature of electron/hole tunneling across the depletion layer.[16] It is possible that a LBMO film of 0.5 nm cannot build up an interfacial barrier that is high and thick enough to prevent the charge tunneling. The ideality factor reduces rapidly from ~2.3 to ~1.1 as the film thickness increases from 0.5 to 1 nm, accompanying a significant weakening of its temperature dependence. This is an indication of the transformation from quantum tunneling to thermoionic emission for the electronic transport.

Figure 4(b) presents the saturation current I_s as a function of reciprocal temperature, obtained by extrapolating the log I-V relation to $V\rightarrow 0$. As well established, $I_s=A^*T^2\exp(-\Phi_B/k_BT)$ for the Schottky junction, where A^* is the Richardson constant, Φ_B the interfacial barrier. Based on this relation, the interfacial barrier can be obtained. The inset in Fig. 4(b) shows the interfacial barrier as a function of film thickness. Φ_B varies between ~0.5 and

~0.6 eV, showing a slight reduction in the junction of $d=1$ nm. The interfacial barrier of the junction of 0.5 nm cannot be obtained in this way because of the severe electric leakage. Similar results are obtained for the LCMO/STON junctions, for which the tunneling process emerges below 1 nm. However, the thickness dependence of the interfacial barrier is slightly strong (not shown). Here the manganite junctions have been treated as Schottky junctions, which is acceptable because the depletion layer mainly forms in STON as shown below.

For a deep understanding of the experimental results, an analysis of the depletion layer of the junction may be helpful. Noting the fact that the semiconductor theory has provided a satisfactory description for the rectifying behaviors of the manganite junctions, we use the formulae for the conventional heterojunctions to estimate the depletion width[16]

$$d_1 = \left[\frac{2N_{D2}\varepsilon_1\varepsilon_2\varepsilon_0 V_D}{qN_{A1}(\varepsilon_1 N_{A1} + \varepsilon_2 N_{D2})}\right]^{1/2}, \quad (1)$$

$$d_2 = \left[\frac{2N_{A1}\varepsilon_1\varepsilon_2\varepsilon_0 V_D}{qN_{D2}(\varepsilon_1 N_{A1} + \varepsilon_2 N_{D2})}\right]^{1/2}, \quad (2)$$

where d_1 (d_2) is the depletion layer thickness of LBMO/LCMO (STON), ε_0 is the permittivity of the vacuum, ε_1 and ε_2 are the permittivity of LBMO/LCMO and STON, respectively, N_{A1} (N_{D2}) is the carrier content in LBMO/LCMO (STON), and $V_D \approx \Phi_B$ is the diffusion potential. A direct calculation gives $d_1=0.03$ nm and $d_2=39$ nm adopting the parameters of $\varepsilon_0=8.85\times10^{-12}$ F/m, $\varepsilon_1=20$, $\varepsilon_2=100$, $N_{A1}=5.7\times10^{27}$ m^{-3}, $N_{D2}=4.3\times10^{24}$ m^{-3}, and $V_D=0.6$ eV. Here N_{A1} and N_{D2} are the nominal carrier contents of LBMO (LCMO) and STON, respectively. The manganite is generally insulating in the near boundary region. The electronic structure is believed to be different from that of the bulk. As a consequence of enhanced lattice distortions, the actual carrier content may be obviously low. To show the effects thus produced, we also calculated the depletion width assuming that, for example, only 10% of the nominal holes survive, and obtained $d_1=0.3$ nm and $d_2=38.5$ nm. Considering the fact that the dielectric constant can be severely depressed by the built-in electric field, here the dielectric constant of STON was set to 100, instead of 300 of $SrTiO_3$.[17] The meanings of these results are twofold. The first one is that the depletion layer in LBMO (LCMO) is extremely thin, which is the basis to ascribe the manganite junction to Schottky junction, and the second one is that the depletion width in STON is insensitive to the hole content of LBMO (LCMO). It is clear that although the films are ultrathin, they, except for the film of 0.5 nm, are still much thicker than d_1. This explains the formation of the junction with a good rectifying character. Although the actual situations in the manganite junction may be somewhat different, the depletion layer in the manganite film could be rather thin. For the junction of 0.5 nm, the depletion layer may not be well developed. As a result, the electron tunneling across the junction dominates its transport behavior.

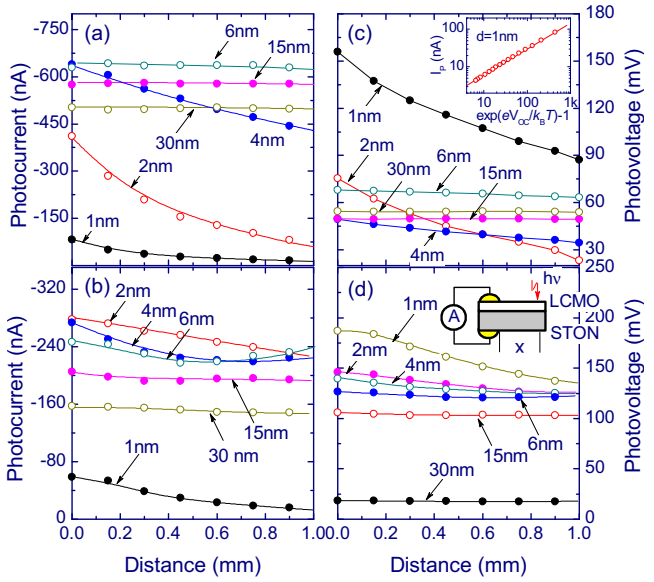

FIG. 5. (Color online) Photocurrent as a function of the lateral distance between electrode and laser spot for the LBMO (a) and LCMO (b) junctions, measured at the ambient temperature. The corresponding photovoltage is shown in (c) and (d). The inset pot in (c) shows the I_p-V_{oc} relation and in (d) a schematic diagram for the experiment setting. Solid lines are guide for the eye.

IV. PHOTOELECTRONIC PROPERTIES

The I-V characteristics describe the transport behavior of the thermally equilibrium charge carriers, and the film thickness in this case takes effects via affecting interfacial barrier and depletion width. However, for the photoelectric process, film thickness may influence the number as well as the diffusion of the extra charge carriers as will be seen below. To get the information on the nonequilibrium charge carriers, the short-circuit photocurrent, I_P, and open-circuit voltage, V_{oc}, were measured as light spot sweeps along the centerline of the rectangular-shaped manganite film. Figures 5(a) and 5(b) show the photocurrent as a function of the distance (x) between electrode and laser spot for the LBMO and LCMO-based junctions, respectively, measured at the ambient temperature. The corresponding photovoltage is shown in Figs. 5(c) and 5(d). The inset in Fig. 5(d) is a schematic diagram for the experiment setting. As expected, I_P takes the maximal values when the laser spot and Cu electrode locate side by side without any gap or overlap, and undergoes a rapid decrease as the light sweeps across the film surface. The maximal and minimal photocurrents are ~82 nA/mm^2 and ~15 nA/mm^2 for, for example, the LBMO/STON junction of $d=1$ nm, appearing at the electrode-laser distance of ~0 mm and ~0.9 mm, respectively. A general feature of the photocurrent is its strong dependence on film thickness. First, I_p displays a steep increase with d for the thin film junctions, and decreases smoothly for the thick film junctions. Second, the I_p decaying with x weakens gradually with the increase in film thickness, and a constant photocurrent is obtained in the junctions of $d>6$ nm. A strong dependence of the photocurrent on film thickness is obvious. Essentially similar I_p-d relations are observed for the LCMO/STON junctions, though the photocurrent is obviously low. Similar to I_P, V_{oc} takes the maximal values when the laser spot and

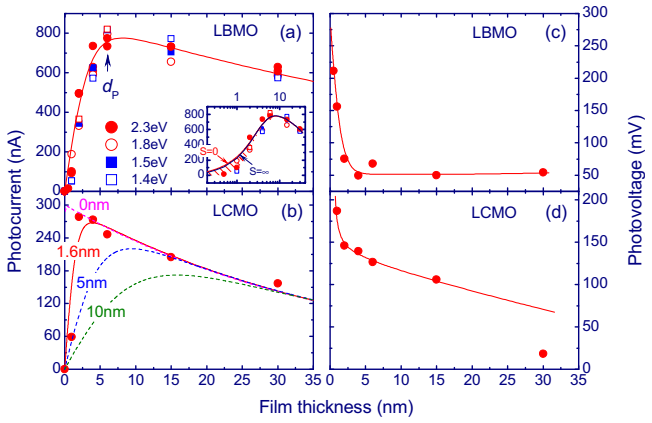

FIG. 6. (Color online) Maximal photocurrent as a function of film thickness for the LBMO (a) and LCMO (b) junctions (symbols). For LBMO/STON, other three sets of data collected under the lasers of 660, 780, and 850 nm are also presented, after a proper scaling, for comparison. Solid lines are theoretical results obtained adopting the parameters of $\alpha=1.4\times10^5$ cm^{-1} and $L=3.5$ nm (LBMO) and $\alpha=2.5\times10^5$ cm^{-1} and $L=1.5$ nm (LCMO) for $S=0$. Results for $S=\infty$, which are nearly overlap with that for $S=0$ after adjusting L to 1.8 nm (LBMO) and 0.9 nm (LCMO) are presented in the inset plot. The inset in (a) is a semilog plot of the I_p-d curves. Shaded area marks the difference between the calculated and detected results. Dashed lines in (b) represent the theoretical I_p-d relations corresponding to diffusion distances marked by the numbers. The corresponding V_{oc}-d relations are shown in (c) and (d).

the electrode nearly overlap, but undergoes a less rapid decrease as the light sweeps away from electrode. It is interesting to note the well linear relation between I_P and $\exp(eV_{oc}/k_BT)-1$ [inset in Fig. 5(c)], which is a typical feature of Schottky diodes.[14]

To get a clear picture on the thickness effect, the I_P-d and V_{oc}-d relations are further analyzed. The magnitude of the photocurrent exhibits a systematic variation with film thickness when x is fixed. Figure 6 presents the maximal photocurrent (photovoltage), corresponding to $x=0$, as a function of film thickness for the LBMO and LCMO junctions (symbols). For LBMO/STON, other three sets of photocurrents collected under the wavelengths of $\lambda=660$ nm and 780 nm, and 850 nm, respectively, are also presented for comparison. As expected, the photocurrent shows a considerable decrease as the wavelength of the laser increases. To clearly show the I_p-d dependence, the photocurrents under the above three wavelengths are normalized by the relation of $I_P(\lambda)I_{p\text{-}peak}(532\text{ nm})/I_{p\text{-}peak}(\lambda)$, where $I_{p\text{-}peak}(\lambda)$ is the peak value of the photocurrent corresponding to the wavelength of λ. I_P is low when d is small, grows steeply with the increase in film thickness, and reaches the maximum around a film thickness of d_P. From LBMO to LCMO, the peak value displays a rapid decrease from ~770 to ~275 nA, accompanying a shift in the peak position from ~6 to ~2 nm. After the I_P peak, a smooth, yet monotonic, photocurrent decrease appears for further increasing d. Although the general I_P-d relation is similar for the two series of samples, difference exists in the detailed I_p-d relation. Compared with that of LBMO/STON, the increase-to-decrease turning is much sharper and the I_p descending with d is slightly rapid for the LCMO/STON junctions. As the film thickness grows from d_p to 30 nm, the photocurrent decreases from ~770 to ~590 nA for LBMO/STON and from ~278 to ~157 nA for LCMO/STON. At a first glance, I_p is likely to decay exponentially with d, which is particularly obvious for the LCMO/STON junctions. On the contrary to the photocurrent, the photovoltage is maximal for the ultrathin film, and undergoes a steep drop with the increase in film thickness. This feature is especially obvious for the LBMO/STON junctions. V_{oc} goes from ~211 to ~51 mV as d grows from 0.5 to 6 nm, and keeps at ~51 mV for further increase in d. Different from LBMO/STON, the photovoltage of LCMO/STON displays a monotonic decrease from ~170 to ~18 mV as d increases.

We repeated the experiments for several times, and obtained similar phenomena. These results clearly show the strong film thickness dependence of the photovoltaic effects in the manganite junctions, especially when the manganite films are ultrathin. Such complex film thickness dependence of the photocurrent deserves special attention. As well established, the photocurrent has a close relation to extra charge carriers. According to the semiconductor theory, electrons/holes in the manganite films can be excited by photons with the energy of $h\nu$ when the condition $\Phi_B<h\nu<E_g$ is satisfied, and the photocarriers entering the depletion region will be swept to the two sides of the depletion layer by internal electric field, forming photocurrent when the junctions are short circuited,[14] where $E_g\approx3.2$ eV, is the band gap of STON.[18] In the present experiments, the laser has the photon energy (1.5–2.3 eV) smaller than E_g. This means that the nonequilibrium carriers contributing to photocurrent come from the manganite film. Noting that the depletion region mainly develops in STON, only the charge carriers entering the STON pole yield the photocurrent.

There are two factors that can affect the photoelectric effect of the junctions. The first one is the variation in the electronic states of the thin film junctions and the second one is film thickness. As is well known, the electronic structure at the near boundary region is generally different from that of the interior for the manganites.[19] This may lead to a growth of the activation energy of the photocarriers, thus a reduction in the photocurrent for thin film junctions, for which the interfacial states play the dominant role. If the I_p reduction totally comes from the downward shift in the valance band, the energy change should be at least ~1.3 eV (The band gap between the valence and conduction bands is ~1 eV for the manganites[20] and the photon energy is ~2.3 eV.) From a simple consideration, we can conclude that the abnormal photocurrent variation could be not ascribed to the effects of the increase in the activation energy of the photocarriers. In fact, if the change in activation energy is the main reason for the I_p drop observed, the I_p-d relation will be different for different photons: As film thickness reduces, the I_p drop may appear earlier under the irradiance of long wavelength lasers, for which the effect of energy shift is much severe. However, the I_p-d relations observed are essentially similar for the photons with the energy from ~1.4 to ~2.3 eV [Fig. 6(a)]. The I_p drop cannot be attributed to the effects of interface disorder either. Provided that the interface disorder is the dominate factor affecting the photoemission process in thin film junctions, its effect should be much stronger for LBMO/

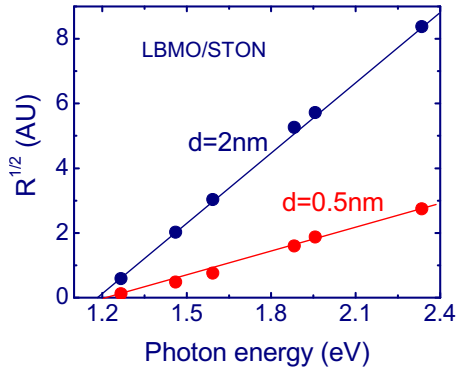

FIG. 7. (Color online) Quantum efficiency as a function of photon energy for the typical LBMO/STON junctions of $d=0.5$ and 2 nm. Solid lines are guides for the eye.

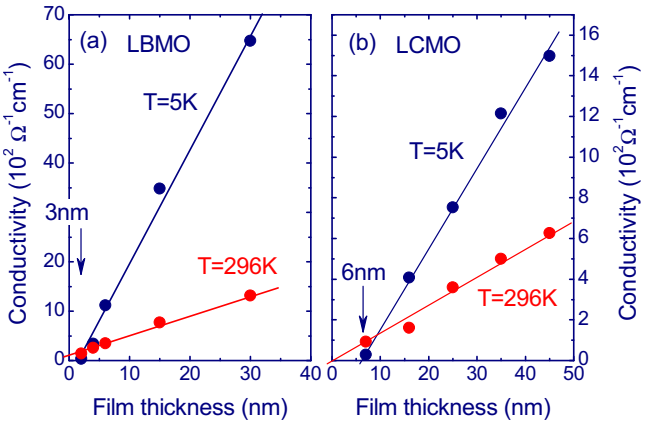

FIG. 8. (Color online) Lateral conductivity of the LBMO (a) and LCMO (b) films, measured at 5 and 296 K. Solid lines are guides for the eye.

STON than for LCMO/STON, appearing when the LCMO film is relatively thick because of the larger lattice mismatch in the latter. However, as shown in Fig. 5, the I_p decrease occurs at ~2 nm for LCMO/STON whereas at ~6 nm for LBMO/STON.

A direct reflection of the activation energy is the interfacial barrier of the junctions. As demonstrated above, the interfacial barrier deduced from the *I-V* analysis shows an independence on film thickness for $d \geq 1$ nm. In general, the interfacial potential obtained in this way is smaller than that derived from the photoemission experiments, due to the occurrence of leakage current.[6] Based on this consideration, we also determined the energy barrier from the photoemission data. Figure 7 illustrates the quantum efficiency ($R \propto I_P h\nu / P$), the number of the photocarriers yielded by each photon, as a function of photon energy for the typical LBMO/STON and LCMO/STON junctions, where P is the power of the laser. The interfacial barrier can be obtained from the $R^{1/2} \propto (h\nu - \Phi_B)$ relation.[21] Φ_B is found to be $\sim 1.2 \pm 0.1$ eV for LBMO/STON of $d \geq 2$ nm, which is similar to that reported for the manganite-based junction,[22] and slightly increases, from $\sim 1.2 \pm 0.1$ eV to $\sim 1.4 \pm 0.1$ eV, as film thickness varies from 2 to 0.5 nm. It is obvious that the change in activation energy should have a random distribution for the thin film junctions, and here only the average change is determined. It is difficult to believe that an increase in ~0.2 eV in activation energy can completely depress the photocurrent.

The photocurrent change has no relation with the abnormal conductive/magnetic property of the ultrathin films either. The lateral resistivity of the LBMO and LCMO films on STON has been studied. The conductive dead layers are ~3 nm and ~6 nm, respectively, in the low temperature limit $T \to 0$. The former is smaller than d_P for LBMO and greater than d_P for LCMO. However, no conductive dead layer is observed at the ambient temperature (Fig. 8), where the photoemission experiments are conducted. As a consequence, the effects of trapped charge re-positioning, if any, should not be strong. These results indicate that the distinctive I_p-d dependence cannot be ascribed to the change in the conductive properties of the manganite films. The I_P drop cannot be ascribed to the change in magnetic state either. Magnetic measurements show that, at the ambient temperature, the LBMO films are in a ferromagnetic state above the thickness of 15 nm and paramagnetic otherwise (not shown), while both the LCMO and LMO films are paramagnetic. Although the two sets of samples are different in magnetic state, their I_P-d curves display similar features.

The second factor affecting the photocurrent is the film thickness. It is obvious that the photocurrent will be zero in the zero d limit, and monotonically increases with film thickness when $d < L$, where L is the diffusion length of the photocarriers. However, when the film thickness is significantly larger than the diffusion distance, only part of the photocarriers excited at the region near the interface has contributions to I_p. In this case, a monotonic growth for $d < L$ and an exponential decrease for $d \gg L$ for the photocurrent are expected, considering the absorption of the laser by the films. This analysis suggests first an increase then a decrease in the photocurrent with the increase in film thickness. It is consistent with the experimental observations.

V. THEORETICAL ANALYSES

Considering the fact that electric leakage may affect the measurements of V_{oc}, in the following we will focus on photocurrent. In fact, there are two processes in the junctions under the irradiance of laser. The first one is the excitation of nonequilibrium carriers. The density of the photocarriers is proportional to the intensity of the laser, which undergoes an exponential decaying described by $\exp(-\alpha z)$ with the distance (z) of the laser in the sample, where α is the absorption coefficient of the light. The second process is the diffusion of these carriers toward the interface of the junction under the driving of the density gradient. It is obvious that only parts of the photocarriers can reach the interface of the junction due to their finite diffusion distance. Based on the standard semiconductor theory, the density of the photocarriers is determined by

$$\frac{d\tilde{n}}{dt} = a\alpha I_0 \exp(-\alpha z) - \frac{\tilde{n}}{\tau} + D\frac{d^2\tilde{n}}{dz^2}, \quad (3)$$

where a is a proportionality constant, I_0 the intensity of incident light, D the diffusion coefficient, and τ the lifetime of the photocarriers. This equation has a generic solution of the form

$$\tilde{n}(z) = A_1 \exp(-z/L) + A_2 \exp(z/L) + M \exp(-\alpha z), \quad (4)$$

when a stable state has been established ($d\tilde{n}/dt=0$), where

$$A_1 = \frac{[-(\alpha D + S)\exp(d/L) + (S - D/L)\exp(-\alpha d)]M}{(S + D/L)\exp(d/L) - (S - D/L)\exp(-d/L)},$$

$$A_2 = \frac{[-(\alpha D + S)\exp(-d/L) + (S + D/L)\exp(-\alpha d)]M}{(S - D/L)\exp(-d/L) - (S + D/L)\exp(d/L)},$$

$$M = a\alpha I_0 \tau/(1 - L^2\alpha^2),$$

under the boundary conditions

$$-D\frac{d\tilde{n}}{dz}\bigg|_{z=0} = -S\tilde{n} \text{ and } \tilde{n}|_{z=d} = 0,$$

S is a parameter characterizing the recombination rate of the photocarriers at the surface of the film, and $L=\sqrt{D\tau}$, is the diffusion distance of the photocarriers. A direct calculation shows that the experiment results can be well described by Eq. (3) adopting proper parameters (not shown). However, L and S are found to be strongly correlated, and L cannot be exclusively determined because of the lacking of the S data for the manganite films. A brief discussion can give us an idea of the effect of S on I_p. It is obvious that the I_p drop will be accelerated by a finite S noting the closeness of the film surface to interface when d is lowering. In this picture, a S value larger (smaller) than the actual one will cause a underestimation (overestimation) of the diffusion distance. This means a monotonic decrease in L as S grows, and the actual diffusion distance will be $L(S=\infty)<L<L(S=0)$.

For two limiting situations of $S=0$ and ∞, Eq. (3) can be simplified to

$$I_P = -D\frac{d\tilde{n}}{dx}\bigg|_{x=d} \propto \begin{cases} \dfrac{-\alpha + \sinh(d/L)\exp(-\alpha d)/L}{\cosh(d/L)} + \alpha\exp(-\alpha d) & \text{for } S=0 \\ \dfrac{-1 + \cosh(d/L)\exp(-\alpha d)}{L\sinh(d/L)} + \alpha\exp(-\alpha d) & \text{for } S=\infty \end{cases}. \quad (5)$$

As shown in Figs. 6(a) and 6(b), Eq. (5) provides an excellent description for the experiment results adopting the absorption coefficients of $\sim 1.4\times10^5$ cm^{-1} (LBMO) and $\sim 2.5\times10^5$ cm^{-1} (LCMO), and the diffusion distances of $\sim$3.5 nm or 1.8 nm and $\sim$1.5 nm or 0.9 nm when setting S to 0 or ∞. This implies 1.8 nm $<L<$ 3.5 nm for LBMO and 0.9 nm $<L<$ 1.5 nm for LCMO. It is interesting that although L is S-dependent, it is relatively insensitive to L. Of course, the interface disorder in thin film junctions may also play a role in affecting I_p. It makes the photocurrent observed lower than that given by Eq. (3). This effect is especially obvious for the junctions of $d<2$ nm [inset in Fig. 6(a)]. However, the diffusion distance is the determinative factor that affects photocurrent.

The maximal diffusion distance deduced is $\sim$3.5 nm. In general, the manganite films are fully strained within 10 nm.[23] This eliminates the dependence of L on d when the latter is small. As we know, the I_p-d relation is mainly determined by L when d is small and by α when $d \gg L$. It is therefore a reasonable assumption that L is constant for the films. We noted that the absorption coefficients of the bulk $LaMnO_3$ are $\sim 0.85\times10^5$ cm^{-1} and $\sim 1.1\times10^5$ cm^{-1} for the wavelength of 532 nm and 660 nm, respectively.[24] Considering the difference between LBMO (LCMO) and $LaMnO_3$, the deduced $\alpha \approx 2.4\times10^5$ cm^{-1} is plausible.

The above analysis reveals the important role of the finite diffusion distance in limiting the photocurrent. Based on it, we can propose a scenario for the internal photoemission process: The photocurrent is low in thin film junctions because of the small number of photocarriers, though the laser intensity is strong near the interface. For thick film junctions, in contrast, although the total number of the excited carriers is large, most of the electrons and holes are recombined before reaching the interface, and only the carriers within L from the interface contribute to I_P. The carrier number is the main factor affecting the photocurrent when the light loss is not severe. In this case I_P shows a monotonic growth with d as occurring for $d<6$ nm for LBMO. However, when the film is thick, the number of the photocarriers near the interface is greatly reduced due to the strong intensity loss of the laser. As a result, the photocurrent is decreased.

The diffusion distance is the longest in the LBMO films and considerably low in the LCMO films. This is understandable noting the different lattice strains in the two series of films. These results show that the diffusion distance of the photocarriers in the manganites is extremely short, only a few nanometers in general. Adopting the mobility of $\mu \approx 1$ mm^2/V s for the manganite films at the ambient temperature,[20] we obtained the lifetime $\tau=L^2/D\approx0.4$ ns, where $D=\mu k_B T/e$ with e being the electron charge. As reported, the mean free path of electrons in the manganite in the high conductive state is the order of 1 nm in magnitude.[25] It may be even smaller at higher temperatures, where carrier scattering is strong. A diffusion distance of a few nanometers

is plausible. Because of the extremely short diffusion distance and the sensitivity of the I_P on L, the photovoltaic effect could be a potential probe for interfacial state. Any processes taking place around the interface, such as charge reconstruction/ordering and spin rearrangement, are expected to have a sizable response in photocurrent/photovoltage.

As a supplement, we would like to point out that the diffusion distance obtained here could be an upper limit for L. In Fig. 6(b) we present the theoretical I_P-d relations corresponding to different diffusion distances (after proper normalizations). The photocurrent exhibits a monotonic increase with the decrease in film thickness in the zero-L limit, and the I_P drop is a signature of finite L. Provided that the sudden drop at d_P is caused by the variation in the electronic structure of ultrathin films instead of finite diffusion distance, the actual L could not exceed that derived from Eq. (5) because of the absence of L-relevant I_P drop above d_P. Based on the above analyses, we believe that the mains effects on I_p in thin film junctions come from the change in film thickness, while the energy level shift in the charge carriers acts as a disturbance.

As experimentally shown, the sudden change in rectifying properties occurs from 0.5 to 1 nm, the latter could be the threshold thickness for the establishment of a well developed depletion layer that and depress electron tunneling. According to the lateral transport behavior of the films, the conductive dead layer is absent at the ambient temperature, where the photoelectronic properties of the manganite is studied, and it is ~3 nm (LBMO) or 6 nm (LCMO) at the temperature of 5 K. In contrast, the photoelectronic experiments suggest a diffusion distance of <3.5 nm for the photocarriers. Three different physical processes have three different character lengths.

VI. SUMMARY

In summary, the rectifying and photoelectronic properties of the $La_{0.67}Ba_{0.33}MnO_3/SrTiO_3$:Nb junctions with the film thickness from d=0.5 nm to 30 nm have been systematically studied. It is found that the electronic transport of the junction is dominated by quantum tunneling or thermoionic emission when film thickness is below or above 1 nm. The rectifying ratio and ideality factor, correspondingly, experience a sudden change as film thickness grows from 0.5 to 1 nm and a smooth variation with film thickness above 1 nm. The threshold film thickness for the establishment of a mature depletion layer is, therefore, 1 nm. The photoemission properties of the junctions also exhibit a strong dependence on film thickness. As experimentally shown, the photocurrent vanishes in the zero thickness limit, and grows rapidly with the increase in film thickness until d=6 nm, where a maximal photocurrent of ~770 nA/mm^2 under the irradiance of the laser of 5 mW and 532 nm is obtained. After this maximum, an increase-to-decrease turning appears with further increasing film thickness. Taking into account the finite diffusion distance of the photocarriers and the strain-enhanced charge trapping in ultrathin film junctions, a theoretical description that well reproduces the experiment results can be obtained, which reveals the severe depression of finite diffusion distance of the extra carriers on photocurrent. The maximal diffusion distance thus obtained is ~3.5 nm. Similar analyses have been performed for the $La_{0.67}Ca_{0.33}MnO_3/SrTiO_3$:Nb junctions, and the corresponding diffusion distance there is ~1.5 nm.

ACKNOWLEDGMENTS

This work has been supported by the National Basic Research of China, the National Natural Science Foundation of China, the Knowledge Innovation Project of the Chinese Academy of Science, and the Beijing Municipal Nature Science Foundation.

[1]For a review, see *Colossal Magnetoresistive Oxides*, edited by Y. Tokura (Gordon and Breach, London, 1999).
[2]H. Tanaka, J. Zhang, and T. Kawai, Phys. Rev. Lett. **88**, 027204 (2001); J. R. Sun, C. M. Xiong, T. Y. Zhao, S. Y. Zhang, Y. F. Chen, and B. G. Shen, Appl. Phys. Lett. **84**, 1528 (2004); N. Nakagawa, M. Asai, Y. Mukunoki, T. Susaki, and H. Y. Hwang, Appl. Phys. Lett. **86**, 082504 (2005).
[3]J. R. Sun, B. G. Shen, Z. G. Sheng, and Y. P. Sun, Appl. Phys. Lett. **85**, 3375 (2004); Z. G. Sheng, B. C. Zhao, W. H. Song, Y. P. Sun, J. R. Sun, and B. G. Shen, *ibid.* **87**, 242501 (2005).
[4]T. Muramatsu, Y. Muraoka, T. Yamauchi, J. Yamaura, and Z. Hiroi, J. Magn. Magn. Mater. **272–276**, E787 (2004).
[5]W. M. Lv, A. D. Wei, J. R. Sun, Y. Z. Chen, and B. G. Shen, Appl. Phys. Lett. **94**, 082506 (2009).
[6]Y. Hikita, M. Nishikawa, T. Yajima, and H. Y. Hwang, Phys. Rev. B **79**, 073101 (2009).
[7]J.-H. Park, E. Vescovo, H.-J. Kim, C. Kwon, R. Ramesh, and T. Venkatesan, Phys. Rev. Lett. **81**, 1953 (1998).
[8]J. Z. Sun, D. W. Abraham, R. A. Rao, and C. B. Eom, Appl. Phys. Lett. **74**, 3017 (1999).
[9]M. Wagenknecht, H. Eitel, T. Nachtrab, J. B. Philipp, R. Gross, R. Kleiner, and D. Koelle, Phys. Rev. Lett. **96**, 047203 (2006).
[10]T. Zhang and M. Dressel, Phys. Rev. B **80**, 014435 (2009).
[11]Y. Wakabayashi, D. Bizen, H. Nakao, Y. Murakami, M. Nakamura, Y. Ogimoto, K. Miyano, and H. Sawa, Phys. Rev. Lett. **96**, 017202 (2006); Y. Z. Chen, J. R. Sun, S. Liang, W. M. Lu, B. G. Shen, and W. B. Wu, J. Appl. Phys. **103**, 096105 (2008).
[12]Y. G. Zhao, J. J. Li, R. Shreekala, H. D. Drew, C. L. Chen, W. L. Cao, C. H. Lee, M. Rajeswari, S. B. Ogale, R. Ramesh, G. Baskaran, and T. Venkatesan, Phys. Rev. Lett. **81**, 1310 (1998).
[13]K. Zhao, K. J. Jin, H. B. Lu, Y. H. Huang, Q. L. Zhou, M. He, Z. H. Chen, Y. L. Zhou, and G. Z. Yang, Appl. Phys. Lett. **88**, 141914 (2006).
[14]S. M. Sze, *Physics of Semiconductor Devices*, 2nd ed. (Wiley, New York, 1981).
[15]J. Blasco, J. García, J. M. de Teresa, M. R. Ibarra, P. A. Algarabel, and C. Marquina, J. Phys.: Condens. Matter **8**, 7427 (1996).
[16]B. L. Sharma and R. K. Purohit, *Semiconductor Heterojunctions* (Pergamon, Oxford, 1974).
[17]S. Suzuki, T. Yamamoto, H. Suzuki, K. Kawaguchi, K. Takahashi, and Y. Yoshisato, J. Appl. Phys. **81**, 6830 (1997); T. Yamamoto, S. Suzuki, K. Kawaguchi, and K. Takahashi, Jpn. J. Appl. Phys., Part 1 **37**, 4737 (1998).
[18]M. Cardona, Phys. Rev. **140**, A651 (1965); B. Reihl, J. G. Bednorz, K. A. Müller, Y. Jugnet, G. Landgren, and J. F. Morar, Phys. Rev. B **30**, 803 (1984).
[19]H. Y. Hwang, S.-W. Cheong, N. P. Ong, and B. Batlogg, Phys. Rev. Lett. **77**, 2041 (1996).
[20]J. M. D. Coey, M. Viret, and S. von Molnár, Adv. Phys. **48**, 167 (1999).
[21]R. H. Fowler, Phys. Rev. **38**, 45 (1931).
[22]M. Minohara, Y. Furukawa, R. Yasuhara, H. Kumigashira, and M. Oshima, Appl. Phys. Lett. **94**, 242106 (2009).
[23]G. Y. Gao, S. W. Jin, and W. B. Wu, Appl. Phys. Lett. **90**, 012509 (2007).
[24]K. Murakami, T. Yamauchi, A. Nakamura, Y. Moritomo, H. Tanaka, and T. Kawai, Phys. Rev. B **73**, 180403(R) (2006).
[25]Q. A. Li, K. E. Gray, and J. F. Mitchell, Phys. Rev. B **63**, 024417 (2000).